Metasurface-Driven Beam Steering Antenna for Satellite Communications

Foez Ahmed*, Khushboo Singh, Karu P. Esselle†, and Dushmantha Thalakotuna
School of Electrical and Data Engineering, University of Technology Sydney (UTS), NSW, Australia.
*foez.ahmed@student.uts.edu.au; †karu@ieee.org

***Abstract*—A metasurface-driven 3D beam-scanning (elevation, azimuth or both) antenna solution is presented in this paper. A pair of novel phase gradient metallic metasurfaces (PGMMs) is designed using the near-electric field phase transformation method operating in the Ku-band. Rotating PGMMs independently atop a static, fixed beam base antenna will enable wide-angle beam-steering in both azimuth and elevation planes. A prototype is made and tested to validate the predicted results. The measured results exhibit excellent beam scanning performance with the highest elevation angle of $\pm 38^\circ$ and a full 360° in the azimuth. This beam-steering approach does not rely on active radio-frequency components. Moreover, the proposed metasurface obviates costly dielectrics, reducing additional cost and weight, and is suitable for stressed environmental conditions such as high-power systems and inter-satellite or deep-space communication systems.**

***Index Terms*—Beam-steering/scanning, dielectric-free, high-gain, high-power, inter-satellite, metal, metasurface, near-field transformation, passive, phase-gradient device, phase-shifting surface, satellite communication.**

I. Introduction

Highly directive beam-steering antenna systems have been at the pivot of an extensive range of applications in space, land and water [1]–[3]. Such antenna technology can provide interference-free, power-saving, and highly secured seamless end-to-end communication independent of the satellites' orientation [4]–[6]. In recent years like defence, satellite communication has also been greatly interested in many non-military applications. This elevates the demand for high-performance antenna technologies at an extremely low cost. In addition, the antenna system must be light, low-profile, low-power driven and easy to manufacture to be compatible with mass-market production [7].

Various technologies have been adopted to achieve beam-steering antennas in the literature. For example, mechanically fully rotatable reflectors, active electronically phased arrays, and reflect/transmit arrays are the conventional ways of steering the antenna beams [8]–[11]. Despite having some merits, these antenna systems are subject to physical and electrical limitations. For example, some of them are heavy and bulky, and others require a lot of 3D or lateral area to perform beam-steering functions. Due to active components and feed networks, arrays are lossy. Some techniques are only feasible for the high-end user due to high production costs [12], [13]. Due to cryogenic temperature and high radiation, the dielectric-based architecture further prohibits deployment in deep space networks (DSNs) or inter-satellite communication systems. Such extreme conditions can alter the dielectric properties or damage the materials; even dielectric properties are not yet known [14].

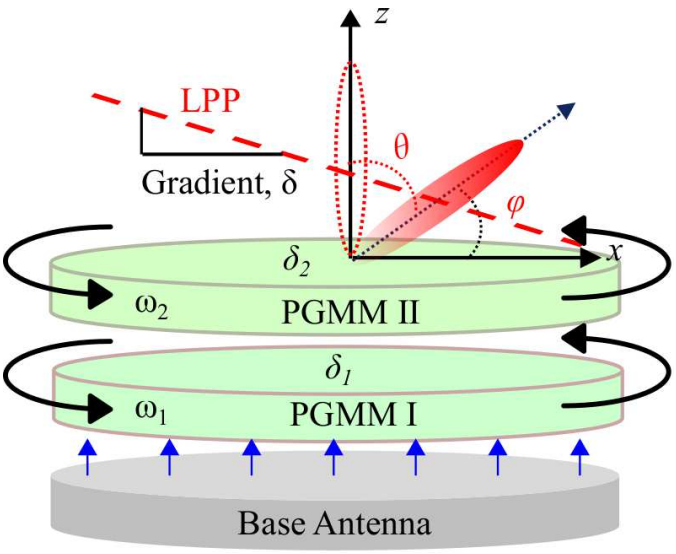

Fig. 1. Beam-steering antenna configuration using a pair of phase gradient metallic metasurfaces.

All-metal architectures could be a possible choice to address those challenges. Metals are cheap and can withstand extreme environmental conditions. Therefore, our primary concern is to avoid the dielectric entirely and build the metasurface with only metal to address those challenges. The near-field meta-steering (NFMS) strategy in developing beam steering antenna systems was introduced in [15] for the first time. However, the metasurfaces proposed in [15] are multilayered metal patches printed on dielectrics. In this method, two metasurfaces are positioned in a base antenna's near-field area and separately rotated to direct the beam in the elevation and azimuth planes. The NFMS system provides some significant advantages, including a simple design strategy, low profile, high electrical performance, low power requirements, and low cost.

This work was supported in part by the Australian Research Council (ARC) discovery grant and in part by UTS FIET seed grant to Karu P. Esselle.

978-1-6654-8237-0/22/$31.00

The rest of this paper is ordered as follows. The beam-steering method is explained in Section II. The design strategy of the phase gradient metallic metasurfaces is discussed in Section III. Section IV presents the predicted and measured antenna performance. Section IV summarizes the paper.

II. Beam-Steering Method

The NFMS antenna configuration is shown in Fig. 1. The antenna comprises a feed and a pair of highly transparent phase gradient metallic metasurfaces (PGMMs) stacked over the feed. PGMM I and II have linear phase progression in their output plane. They are typically identical if the feed radiates plane waves. Otherwise, PGMM I needs to be customized to make it compatible with the feed to simultaneously provide linear phase progression and phase error correction. The corresponding orientation and beam tilting angles of PGMM I and II are denoted by ω_1, ω_2, δ_1, and δ_2, respectively. Here, it is worth mentioning that the beam tilting angles (δ_i) defined by each metasurface can be fixed at the design level of PGMMs using (1), where $\Delta\phi$ represents the progressive phase steps, Δd stands for cells' spacing in the array, and λ_0 is a free-space wavelength. In such a configuration, the feed is static, and PGMM I and II are independently rotated to scan the beam in the azimuth and elevation plane continuously. The beam peaks (θ, ϕ) at elevation and azimuth planes can be estimated analytically using (2) and (3) [16].

$$\delta_{i/j} = sin^{-1}\left(\frac{\Delta\phi}{2\pi} \times \frac{\lambda_0}{\Delta d}\right) \tag{1}$$

$$\theta = \sin^{-1}\left\{\frac{1}{k}\sqrt{\delta_1^2 + \delta_2^2 + 2\delta_1\delta_2\cos\left(\omega_1 - \omega_2\right)}\right\} \tag{2}$$

$$\phi = \tan^{-1}\left(\frac{\delta_i}{\delta_j}\right) = tan^{-1}\frac{\delta_1\sin(\omega_1) + \delta_2\sin(\omega_2)}{\delta_1\cos(\omega_1) + \delta_2\cos(\omega_2)} \tag{3}$$

For a numerical example, let us assume that both PGMMs have identical beam tilt angels, i.e. $\delta = \delta_1 = \delta_2 = 19.5°$. If PGMM II is rotated anticlockwise from $\omega_2 = 30$ to $180°$ in the step of $30°$ while PGMM I is static and its linear phase progression is aligned with the base antenna axis, the beam will move both in elevation and azimuth planes. Using (2) and (3), the beam locations in the elevation and azimuth planes are estimated, and numerical values are listed in Table I. Similarly, the beam can be steered either at the azimuth or elevation plane only by synchronous co-rotation or counter-rotation of the metasurface pair.

III. Beam Tilting Metallic Metasurface

As discussed in Section II, the PGMMs are the key components to steer the beam in the NFMS antenna system. They consist of supercells, and each supercell is composed of unique cells (meta-atoms). For example, the PGMMs are designed to steer the antenna beam at 19.5° offset. Therefore, according to (1), a supercell of six distinct cells is needed if the progressive phase step ($\Delta\phi$) is 60° and $\Delta d = 12$ mm. The front view of a supercell configuration made of such six cells is shown in Fig. 2 (a). The supercell size is $3\lambda_0$, and each cell's periodicity (P) is $\lambda_0/2$, where λ_0 is the operating wavelength at 12.5 GHz. They are made of four identical 0.3 mm thin sheets of metal, as shown in Fig. 2 (b). Each metal sheet has a cross slot cut in the centre, and a $\lambda_0/4$ air gap separates each metal layer. The width of all slots is fixed to 0.5 mm, and the middle and edge slot lengths are varied to tune the desired phase and magnitudes of the transmitting electric fields. Cells were simulated in CST Microwave Studio (CST MWS) under periodic boundary conditions to choose the required cells. The transmission coefficients of the selected best six cells are plotted in Fig. 3. A linear phase progression of 60° is observed, with the least transmission magnitude of -0.9 dB. The respective middle and edge slots' dimensions of cell 1 to 6 are (in mm): (8.7, 2.9), (7.5, 3.7), (8.0, 3.1), (8.4, 2.6), (9.8, 1.4), and (9.1, 2.8).

The PGMMs are then formed by arranging the supercells in a 2D array, as pictorially demonstrated in Fig. 4. In this strategy, the supercell described in Fig. 2 is periodically arranged along the x-axis of linear phase progression and the orthogonal axis (y-axis), where the phase will be invariant. Such two identical PGMMs can move the beam in the elevation and azimuth planes following the method discussed in Section II. However, the horn used to demonstrate the beam steering concept here does not radiate plane waves; hence PGMM I should be redesigned to operate in dual modes for simultaneous phase correction and linear phase progression. The design strategy of phase correcting metasurface and dual-mode metasurface was explained at length in [17]–[19] and is

TABLE I
Beam peak positions while PGMM I is static and PGMM II is rotated anticlockwise.

PGMM I and II (Angular positions)		Beam Pointing Positions	
ω_1 (°)	ω_2 (°)	θ (°)	ϕ (°)
0	30	38.6	15
0	60	34.6	30
0	90	28.3	45
0	120	20.0	60
0	150	10.4	75
0	180	0.0	90

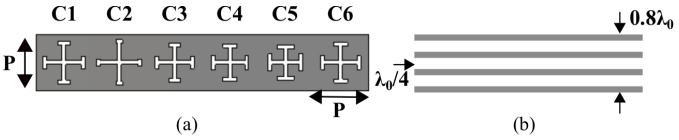

Fig. 2. Supercell topology: (b) top view shows the corresponding unit-cell arrangement, and (a) side view of four thin metal layers.

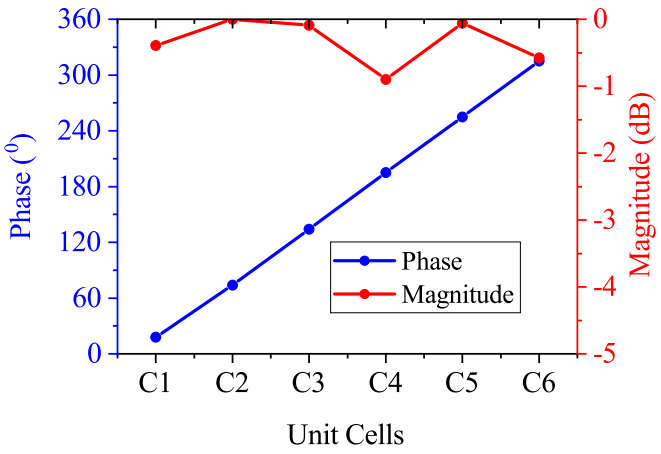

Fig. 3. Transmission coefficients of the best six cells to form the supercell.

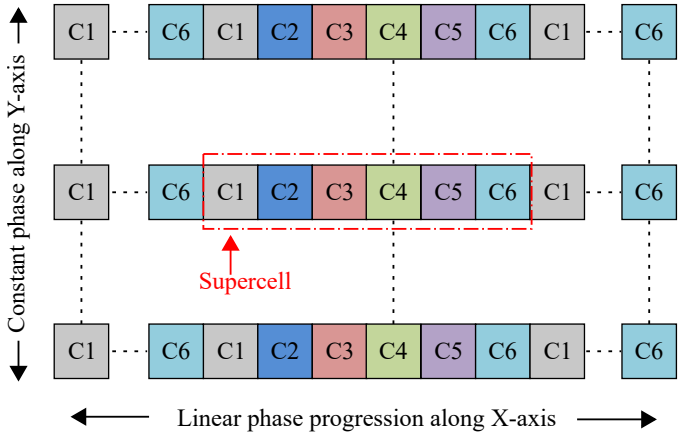

Fig. 4. Supercell arrangement to form a PGMMs extended in a 2D plane.

not reiterated for brevity.

A conical horn made of 3D printing facilities is considered to demonstrate the beam steering concept using a pair of PGMMs. The horn's circular aperture diameter and flare height were fixed to $6\lambda_0$ and $3.125\lambda_0$, respectively, to get the optimum performance. Therefore, two supercells along the x-axis and 12 repeats along the y-axis are necessary to fill the whole horn's aperture. Circular-shaped PGMMs similar in size to the horn's aperture were modeled following the design strategy demonstrated in Fig. 4. The PGMMs were fabricated using laser-cut technology. The minimal metal was ablated from thin metal sheets, hence retaining enough mechanical strength to hold it up without any external supports. The top views of fabricated PGMM I and II are shown in Fig. 5 (a) and (b), respectively. Such four identical metal sheets for each PGMM are then stacked vertically using $\lambda_0/4$ nylon spacers to form the PGMMs, as shown in Fig. 5 (c). The assembled four-layered PGMM I and II are then stacked over the horn to complete the beam-steering antenna prototype, as demonstrated in Fig. 1. The air gap between the horn and

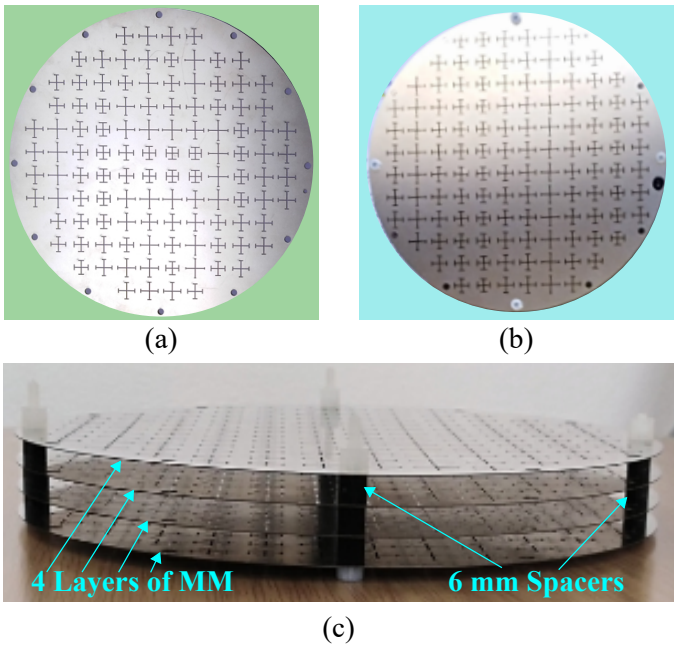

Fig. 5. Photograph of fabricated (a) PGMM I, (b) PGMM II and (c) an assembled four-layered phase gradient MM.

PGMM I is $\lambda_0/24$, whereas $\lambda_0/6$ nylon spacers separate two metasurfaces. Including feed and two PGMMs, the overall antenna height is around $4.9\lambda_0$. Each PGMM is $0.8\lambda_0$ thick and weighs 143.3 g only.

IV. Resutls

The antenna performance was verified in two phases. The horn antenna was first modeled and measured using the PGMM I alone. Then, the whole antenna system (horn with PGMM I and II) was tested to evaluate the beam-steering performance in elevation and azimuth planes.

A. Horn with PGMM I

This measurement system fixed the horn, and PGMM I was rotated at ω_1 =0, 90, 180 and 270°. For each case, the antenna input impedance and realized gain were measured over a wideband and plotted in Fig. 6. The VSWR indicates negligible coupling effects between the horn and PGMM I. In the worst-case scenario, the impedance matching bandwidth and 3-dB gain bandwidth are 16% (from 11.5 GHz to 13.5 GHz) and 8.8% (from 11.9 GHz to 13.0 GHz), respectively. At 12.4 GHz, the highest peak gain of 20.07 dBi is attained, and for four different angular orientations of the PGMM I, the gain variation at that frequency is just 0.57 dBi. The predicted 3D far-field radiation patterns at design frequency 12.5 GHz are shown in Fig. 7. In all cases, the beam is well directed at 19.5° in the elevation plane, as expected, and side lobe levels (SLLs) are at least 12.4 dB below the main lobe. Overall, it validates the 360° beam scanning concept in the azimuth plane by turning PGMM I.

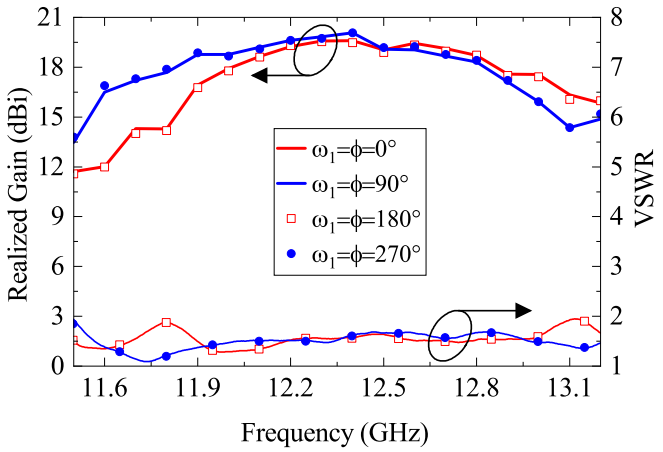

Fig. 6. Measured realized gain and VSWR when the horn is statice and PGMM I is rotated atop the fixed-beam horn.

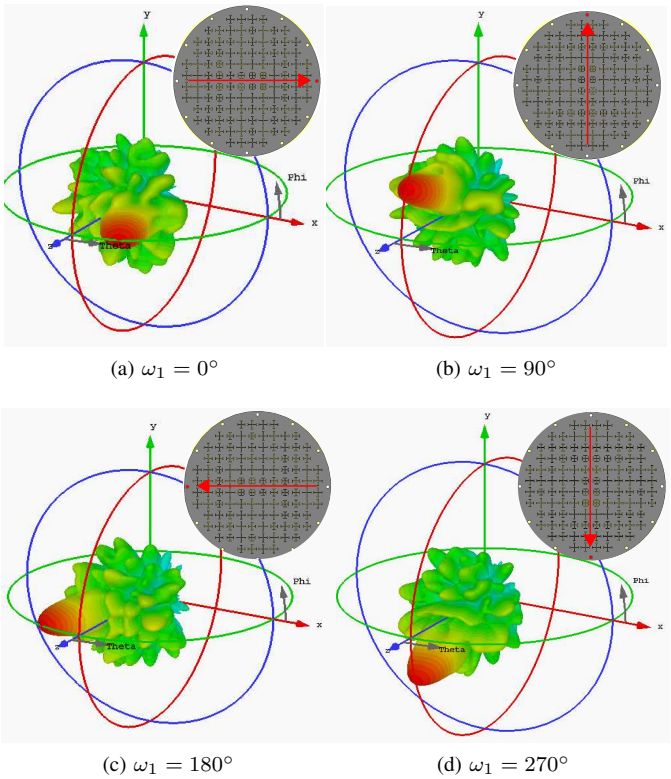

(a) $\omega_1 = 0°$ (b) $\omega_1 = 90°$

(c) $\omega_1 = 180°$ (d) $\omega_1 = 270°$

Fig. 7. Predicted 3D beam patterns and their positions when the horn is static and PGMM I is rotated atop the fixed-beam horn.

B. Horn with PGMM I and PGMM II

This measurement system fixed the horn and PGMM I at $\omega_1 = 0$, and PGMM II was turned counterclockwise around the z-axis at a step of 30° from $\omega_2 = 30°$ to 180°. The antenna input impedance, realized gain and far-field patterns were measured for each case. The antenna input impedance bandwidth is more than 8.8%, and the 3-dB gain bandwidth is at least 700 MHz, irrespective of the rotation of PGMM II.

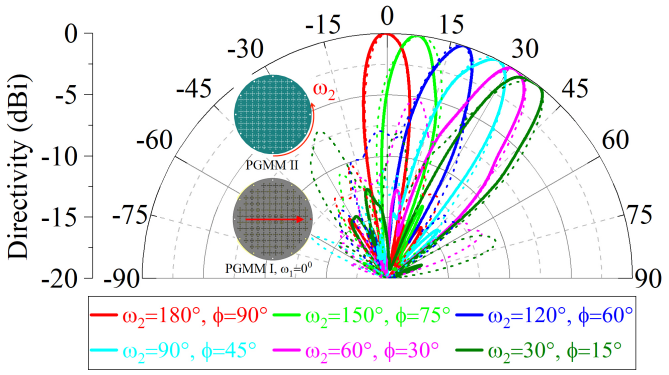

Fig. 8. Measured (solid curves) and simulated (dotted curves) far-field radiation pattern cuts at 12.5 GHz. PGMM I is static, and PGMM II is rotated from $\omega_2 = 30°$ to 180° in steps of 30°.

The 2D far-field patterns measured at design frequency 12.5 GHz in the elevation plane are plotted in Fig. 8. The predicted pattern cuts are also included for a fair comparison. There is good agreement between measured and predicted results. As expected, the beam peaks are highly directive and well pointed for all angular positions (ω_2) of PGMM II, while PGMM I is fixed at $\omega_1 = 0$. It can be observed that the measured SLLs are reasonably low for all beam-steering scenarios, which is at least 12.6 dB below the main lobe. The proposed antenna prototype can steer the beam in the elevation plane from +38° to -38° over an upper hemisphere with excellent pattern quality. Both predicted and measured results validate the 3D beam-steering concept using a pair of lightweight PGMMs.

V. Conclusion

A low-cost, low-profile, and lightweight 3D beam-scanning antenna system has been successfully built and experimentally tested using new planar and passive PGMMs. The proposed PGMMs are mechanically robust and obviate the need for additional supporting or costly dielectrics. The antenna can steer the beam from broadside to ±38° without tilting the antenna or using costly and lossy active phase shifters. Its potential for space and high-power applications is increased due to the absence of dielectric, which also significantly decreases the cost and weight of the system.

References

[1] D. G. Lockie, M. Sereno, and M. Thomson, "Spacecraft Antennas and Beam Steering Methods for Satellite Communication System," Jun. 24 1997, united states patent 5,642,122.

[2] X. Flores-vidal, P. Flament, R. Durazo, C. Chavanne, and K. W. Gurgel, "High-Frequency Radars: Beamforming Calibrations Using Ships as Reflectors," *J. Atmos. Ocean. Technol.*, vol. 30, no. 3, pp. 638–648, Mar. 2013.

[3] V. M. Jayakrishnan and D. M. Vijayan, "Performance Analysis of Smart Antenna for Marine Communication," *2nd Int. Conf. Innov. Mech. Ind. Appl. ICIMIA 2020 - Conf. Proc.*, no. Icimia, pp. 88–91, 2020.

[4] E. Amyotte, Y. Demers, M. Forest, L. Hildebrand, and S. Richard, "A review of recent antenna developments at MDA," *2013 7th Eur. Conf. Antennas Propagation, EuCAP 2013*, no. Eucap, pp. 3614–3618, 2013.

[5] M. H. Novak and J. L. Volakis, "Ultrawideband Antennas for Multi-band Satellite Communications at UHF–Ku Frequencies," *IEEE Trans. Antennas Propag.*, vol. 63, no. 4, pp. 1334–1341, apr 2015.

[6] J. Wu, Y. J. Cheng, and Y. Fan, "A Wideband High-Gain High-Efficiency Hybrid Integrated Plate Array Antenna for V-Band Inter-Satellite Links," *IEEE Trans. Antennas Propag.*, vol. 63, no. 4, pp. 1225–1233, apr 2015.
[7] K. P. Esselle, "A Brief Overview of Antenna Technologies for Communications-On-The-Move Satellite Communication Mobile Terminals," in *IEEE Int. Symp. Antennas Propag.*, 2020, pp. 1637–1638.
[8] A. W. Rudge and M. J. Withers, "New Technique for Beam Steering with Fixed Parabolic Reflectors," *Proc. Inst. Electr. Eng.*, vol. 118, no. 7, pp. 857–863, Jul. 1971.
[9] A. I. Zaghloul, O. Kilic, and E. C. Kohls, "System Aspects and Transmission Impairments of Active Phased Arrays for Satellite Communications," *IEEE Trans. Aerosp. Electron. Syst.*, vol. 43, no. 1, pp. 176–186, Jan. 2007.
[10] A. H. Abdelrahman, F. Yang, A. Z. Elsherbeni, and P. Nayeri, "Analysis and Design of Transmitarray Antennas," *Synth. Lect. Antennas*, vol. 6, no. 1, pp. 1–175, jan 2017.
[11] P. Nayeri, F. Yang, and A. Z. Elsherbeni, *Reflectarray Antennas*. Chichester, UK: John Wiley & Sons, Ltd, feb 2018.
[12] C. Henry, "Panasonic Avionics: 'Jury's still out' on Profitability of In-Flight Connectivity," 2017. [Online]. Available: https://spacenews.com/panasonic-avionics-jurys-still-out-on-profitability-of-in-flight-connectivity/
[13] K. P. Esselle, "Mobile satellite communication terminals—State of the art and antenna challenges," in *Proc. 14th Eur. Conf. Antennas Propag.*, 2020.
[14] N. Chahat, B. Cook, H. Lim, and P. Estabrook, "All-Metal Dual-Frequency RHCP High-Gain Antenna for a Potential Europa Lander," *IEEE Trans. Antennas Propag.*, vol. 66, no. 12, pp. 6791–6798, Dec. 2018.
[15] M. U. Afzal and K. P. Esselle, "Steering the Beam of Medium-to-High Gain Antennas Using Near-Field Phase Transformation," *IEEE Trans. Antennas Propag.*, vol. 65, no. 4, pp. 1680–1690, Apr. 2017.
[16] J. Wang and Y. Ramhat-Samii, "Phase method: A more precise beam steering model for phase-delay metasurface based risley antenna," in *URSI Int. Symp. Electromagn. Theory (EMTS)*, 2019, pp. 12–15.
[17] F. Ahmed, M. U. Afzal, T. Hayat, K. P. Esselle, and D. N. Thalakotuna, "A Dielectric Free Near Field Phase Transforming Structure for Wideband Gain Enhancement of Antennas," *Sci. Rep.*, vol. 11, no. 1, pp. 1–13, 2021.
[18] F. Ahmed, M. U. Afzal, T. Hayat, K. P. Esselle, and D. N. Thalakotuna, "Self-Sustained Rigid Fully Metallic Metasurfaces to Enhance Gain of Shortened Horn Antennas," *IEEE Access*, vol. 10, pp. 79 644–79 654, 2022.
[19] F. Ahmed, M. U. Afzal, T. Hayat, K. P. Esselle, and D. N. Thalakotuna, "A Near-Field Meta-Steering Antenna System with Fully Metallic Metasurfaces," *IEEE Trans. Antennas Propag.*, pp. 1–1, 2022, doi:10.1109/TAP.2022.3185502.